Flow Measurement and Instrumentation 82 (2021) 102081

Contents lists available at ScienceDirect

Flow Measurement and Instrumentation

journal homepage: www.elsevier.com/locate/flowmeasinst

Total fractional-order variation regularization based image reconstruction method for capacitively coupled electrical resistance tomography

Yanyan Shi [a,b], Juanjuan Liao [a], Meng Wang [a,*], Yating Li [a], Feng Fu [b,**], Manuchehr Soleimani [c]

[a] Key Laboratory of Optoelectronic Sensing Integrated Application of Henan Province, Department of Electronic and Electrical Engineering, Henan Normal University, Xinxiang, 453007, China
[b] College of Biomedical Engineering, Fourth Military Medical University, Xi'an, 710032, China
[c] Department of Electronic and Electrical Engineering, University of Bath, Bath, BA2 7AY, UK

ARTICLE INFO

Keywords:
Capacitively coupled electrical resistance tomography
Image reconstruction
Total fractional-order variation regularization

ABSTRACT

Compared with electrical resistance tomography, capacitively coupled electrical resistance tomography (CCERT) is preferred since it avoids problems of electrode corrosion and electrode polarization. However, reconstruction of conductivity distribution is still a great challenge for CCERT. To improve reconstruction quality, this work proposes a novel image reconstruction method based on total fractional-order variation regularization. Simulation work is conducted and reconstruction of several typical models is studied. Robustness of the proposed method to noise is also conducted. Additionally, the performance of the proposed reconstruction method is quantitatively evaluated. We have also carried out phantom experiment to further verify the effectiveness of the proposed method. The results demonstrate that the quality of reconstruction has been largely improved when compared with the images reconstructed by Landweber, Newton-Raphson and Tikhonov methods. The inclusion is more accurately reconstructed and the background is much clearer even under the impact of noise.

1. Introduction

Electrical resistance tomography (ERT) is an emerging imaging technique which has received considerable attention in monitoring multiphase flow [1–3]. Compared with other tomographic methods, ERT has advantages of fast response, low cost, non-radiation and non-invasiveness [4,5]. It is able to visualize conductivity distribution. However, electrodes which are performed as sensor in ERT are in contact with the measured medium. As a result, electrode corrosion or electrode polarization occur which affects measurement accuracy. Inspired by capacitively coupled contactless conductivity detection (C^4D), capacitively coupled electrical resistance tomography (CCERT) has been developed [6,7]. It is a non-contact conductivity measurement method with which imaging of conductivity distribution can be also realized. In CCERT, an array of electrodes is installed outside the pipe at equal intervals. Since the electrodes are not contact with the medium in the pipe, the problems of electrode corrosion and polarization in ERT can be avoided. It largely improves the system reliability and reduces the maintenance cost.

It should be remarked that image reconstruction is essential for conductivity reconstruction with CCERT. By processing the measured data, conductivity distribution in the detected region can be visualized with an image reconstruction method. It is known that reconstruction in ERT is mathematically a nonlinear ill-posed inverse problem. To cope with this problem, various methods have been proposed [8–11]. Similar with ERT, it is also a great challenge for imaging of conductivity distribution with CCERT. Up until now, a number of methods have been proposed for image reconstruction in CCERT. In Ref. [12], a hybrid image reconstruction method with the combination of Tikhonov regularization and synchronous iterative reconstruction technique is presented for recovering conductivity distribution. In Ref. [13], image reconstruction in CCERT is implemented by combining Levenberg-Marquardt (L-M) method with synchronous algebraic reconstruction technique. With grey-level distribution of the image obtained by L-M method as the initial iterative value, the reconstruction is realized by employing synchronous algebraic reconstruction technique. In Ref. [14], an image reconstruction method combing linear back projection algorithm with K-means clustering algorithm is proposed. The linear back projection algorithm is used to obtain the original reconstructed image and the K-means clustering algorithm is used to

* Corresponding author.
** Corresponding author.
E-mail addresses: wangmeng@htu.edu.cn (M. Wang), fengfu@fmmu.edu.cn (F. Fu).

https://doi.org/10.1016/j.flowmeasinst.2021.102081
Received 14 May 2021; Received in revised form 10 October 2021; Accepted 9 November 2021
Available online 15 November 2021

obtain grey threshold values. Although some satisfactory results have been acquired, the reconstruction quality is still needed to be improved.

To solve a typical ill-posed inverse problem in electrical tomography, Tikhonov regularization is a classic approach [15]. By adding a smoothing regularization term, the ill-posed problem can be regularized and is converted into a well-posed problem. However, the edge of an image is not well preserved with this method [16]. Comparatively, total variation regularization offers an alternative for edge preservation since it allows solutions with discontinuities [17–20]. The disadvantage is that undesired blocky effect also known as staircasing artifact is yielded [21]. This is due to the fact that this method tends to convert smooth regions of solution into piecewise constant regions during functional minimization [22]. Mathematically, the problem of total variation method can be addressed by introducing higher-order or fractional-order derivatives. The success of these methods has been demonstrated in the field of image processing [23–25]. In this work, a novel image reconstruction method based on total fractional-order variation regularization (TFVR) is proposed for recovering conductivity distribution in CCERT.

The remainder of this work is organized as follows. In section II, the mathematical model of CCERT is presented. The proposed TFVR method is provided in section III. In section IV, numerical simulation and phantom experiment are conducted to demonstrate the effectiveness of the proposed method. Also, comparison work with other reconstruction methods is performed. Section V draws the conclusion.

2. Mathematical model of CCERT

A typical CCERT measurement system is mainly composed of an array of sensor electrodes, a data acquisition and processing unit, and an image reconstruction unit. Fig. 1 shows the arrangement of electrodes in CCERT and its equivalent excitation-measurement circuit. As shown in Fig. 1(a), twelve electrodes are equidistantly equipped around an insulating pipe filled with conductive medium. With one electrode excited by an alternating voltage and one electrode performed as a measurement terminal, an AC path is established between the two electrodes [26]. The equivalent circuit is illustrated in Fig. 1(b). C_{p1} and C_{p2} denote the coupling capacitance between two electrodes while R_m represents the equivalent resistance of conductive medium. Note that the current measured from the detection electrode reflects medium conductivity. Based on the measurement obtained by the data acquisition and processing unit, conductivity distribution is visualized with the image reconstruction unit.

The electrode is excited at the frequency of 500 kHz. Since the wavelength of the excitation signal is much longer than the dimension of the detected region, sensitive field in CCERT is a quasi-static electromagnetic field. Based on Maxwell equations, the relationship between potential distribution and electrical parameters is mathematically described by Ref. [27]:

$$\nabla((\sigma(x,y)+j\omega\varepsilon(x,y))\nabla\psi(x,y))=0 \quad (x,y)\subseteqq\Omega \tag{1}$$

where $\sigma(x,y)$ represents conductivity distribution, $\varepsilon(x,y)$ and $\psi(x,y)$ are respectively spatial permittivity and potential distribution, and Ω denotes the sensing area.

Boundary conditions are expressed by

$$\begin{aligned}&\psi_i(x,y)=V_0 \quad (x,y)\subseteqq\Gamma_i\\&\psi_j(x,y)=0 \quad (x,y)\subseteqq\Gamma_j\\&\frac{\partial\psi_k(x,y)}{\partial n}=0 \quad (x,y)\subseteqq\Gamma_k(k\neq i,j)\end{aligned} \tag{2}$$

where i, j and k are the indexes of excitation electrode, detection electrode and floating electrodes, respectively; V_0 is the sinusoidal excitation voltage; Γ_i , Γ_j , Γ_k represent the spatial locations of excitation electrode, detection electrode and floating electrodes, respectively; n denotes outward unit normal vector.

The current I_{ij} measured on the detection electrode can be obtained by [28].

$$I_{ij}=\int_{\Gamma}J\cdot d\Gamma \tag{3}$$

where J represents current density near the electrode.

The equivalent impedance Z_{ij} between the excitation and detection electrode pairs can be calculated. It is worth noting that only the real part of Z_{ij} represents equivalent resistance between electrodes which reflects conductivity. Therefore

$$\begin{aligned}&Z_{ij}=\frac{V_0}{I_{ij}}\\&R_{ij}=\mathrm{Re}(Z_{ij})\end{aligned} \tag{4}$$

where R_{ij} is the equivalent resistance between electrode pairs i and j.

To mathematically describe forward problem of CCERT, variation of equivalent resistance ΔR against conductivity change is formulated by [29].

$$\Delta R=S\Delta\sigma \tag{5}$$

where S represents sensitivity matrix which reflects the change of resistance caused by conductivity variation in the measured domain.

For simplicity, (5) is rewritten as

$$H=Sg \tag{6}$$

where H represents ΔR and g stands for $\Delta\sigma$.

3. Image reconstruction based on total fractional-order variation regularization

It can be found from (6) that conductivity distribution in the detected region can be calculated once resistance and sensitivity matrix are known. In this paper, a novel total fractional-order variation regularization (TFVR) strategy is proposed for reconstructing conductivity

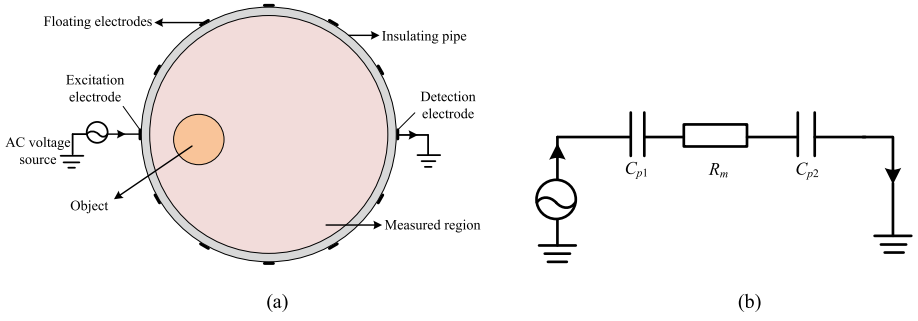

Fig. 1. (a)The sketch of a 12-electrode CCERT sensor (b)Equivalent circuit of an electrode pair.

change against homogeneous distribution in CCERT. To cope with the ill-posedness of reconstruction, a fractional-order regularization term is added to restrict the solution. The proposed TFVR strategy is mathematically modeled as

$$\widehat{g} = \underset{g}{\operatorname{argmin}} \left\{ \frac{\lambda}{2} \|Sg - H\|_2^2 + \|D^p g\|_1 \right\} \tag{7}$$

where $\widehat{g}$ is the estimated optimal conductivity, λ is the regularization parameter used to balance the fidelity term and the regularization term, D^p is the pth order finite difference in which p is the order and D is the gradient operator.

Eq. (7) can be rewritten as

$$\widehat{g} = \underset{g}{\operatorname{argmin}} \left\{ \frac{\lambda}{2} \|Sg - H\|_2^2 + \|w\|_1 \right\}, \quad D^p g = w \tag{8}$$

Due to non-differentiability and nonlinearity, it is still difficult to solve (8) directly and effectively. Therefore, iterative alternating minimization method is introduced to obtain the solution of inverse problem. According to Ref. [30], minimized augmented Lagrangian function of (8) is formulated as

$$\begin{aligned} \min_{w,g} L_A(w,g) = \|w\| - v^{\mathrm{T}}\left(D^p g - w\right) + \frac{\beta}{2}\left\|D^p g - w\right\|_2^2 - \lambda^{\mathrm{T}}(Sg - H) \\ + \frac{\mu}{2}\|Sg - H\|_2^2 \end{aligned} \tag{9}$$

where T denotes the transpose operator, and v, β, μ are the augmented Lagrangian multipliers.

Referring to alternating direction method introduced in Refs. [31] and [32], (9) is decomposed into two simple sub-problems termed as w sub-problem and g sub-problem which are respectively expressed as:

$$\begin{cases} \min\limits_{w} \|w\| - v^{\mathrm{T}}(D^p g_m - w) + \dfrac{\beta}{2}\|D^p g_m - w\|_2^2 \\ \min\limits_{g} \xi_m(g) \triangleq - v^{\mathrm{T}}(D^p g - w_{m+1}) + \dfrac{\beta}{2}\|D^p g - w_{m+1}\|_2^2 - \lambda^{\mathrm{T}}(Sg - H) + \dfrac{\mu}{2}\|Sg - H\|_2^2 \end{cases} \tag{10}$$

For the w sub-problem, its solution is given by

$$w_{m+1} = \max\left(\left\| D^p g_m - \frac{v}{\beta} \right\| - \frac{1}{\beta}, 0 \right) \frac{D^p g_m - \frac{v}{\beta}}{\left\| D^p g_m - \frac{v}{\beta} \right\|} \tag{11}$$

The solution of the g sub-problem is computed by:

$$g_{m+1} = \left(\beta (D^p)^{\mathrm{T}} D^p + \mu S^{\mathrm{T}} S\right)^{+} \left(\left(D^P\right)^{\mathrm{T}} v + \beta (D^p)^{\mathrm{T}} w_{m+1} + S^{\mathrm{T}} \lambda + \mu S^{\mathrm{T}} H \right) \tag{12}$$

Besides, the one-step steepest descent method is adopted to obtain the final solution as:

$$g_{m+1} = g_m - \alpha_m d_m \tag{13}$$

in which the step length is calculated by

$$\alpha_m = \frac{Z_m^{\mathrm{T}} Z_m}{Z_m^{\mathrm{T}} Y_m}$$

where d is the gradient direction of the objective function.

Note that

$$Z_m = g_m - g_{m-1} \text{ and } Y_m = d_m(g_m) - d_m(g_{m+1}) \tag{14}$$

During the iteration, the nonmonotone Armijo condition is required which is expressed as [33].

$$\xi_m(g_m - \alpha_m d_m) \le C_m - \delta \alpha_m d_m^{\mathrm{T}} d_m \tag{15}$$

in which

$$C_{m+1} = \frac{\eta P_m C_m + \xi_m(g_{m+1})}{P_{m+1}}$$

$$P_{m+1} = \eta P_m + 1$$

where η and δ are selected between 0 and 1.

To summarize, the proposed TFVR strategy for image reconstruction in CCERT can be solved by alternating minimization scheme which is tabulated in Algorithm 1.

Algorithm 1: The solution for the proposed TFVR strategy

Input: S, H, m,δ,ρ,η, w_0, g_0.
Initialize: $0 < \delta, \rho, \eta < 1, C_0 = L_A(w_0, g_0)$.
Iterations:
1. While inner stopping condition unsatisfied **do**
2. Compute w_{m+1} using (11);
3. Set α_m through formula (13);
4. While formula (15) unsatisfied **do**
5. Backtrack $\alpha_m = \rho \alpha_m$;
6. End do
7. Compute g_{m+1} by one-step steepest descent method (13);
8. Set C_{m+1} according (15);
9. $m = m+1$
10. End do
Output: g_{m+1}

4. Simulation and experimental reconstruction

4.1. Simulation work

In this section, image reconstruction is conducted for CCERT. It is implemented with Matlab R2016a which is installed on a laptop with Intel Core 3.4 GHz processor and 8 GB RAM. In the simulation, forward problem is solved by Comsol MultiPhysics which is developed based on finite element method and forward solver is the same in all reconstruction methods. A circular region with inner diameter of 50 mm and outer diameter of 54 mm is constructed. Twelve electrodes are equidistantly installed outside the circular region and inclusions are located in the detected area. The conductivity of the background and the inclusions is set to 0.03 S/m and 0.001 S/m, respectively. The circular region is meshed into triangular meshes when solving the forward problem. With an alternating voltage injected to an electrode, equivalent resistance is calculated from another electrode while other electrodes are set to floating potential. There are totally 132 measurement data. The sensitivity matrix is then obtained. Based on the calculated sensitivity matrix and the measured resistance, conductivity distribution is reconstructed with the proposed TFVR method implemented in Matlab R2016a. To reduce the amount of calculation, square mesh is applied in the inverse problem. Note that the number of meshes when solving inverse problem is much smaller than that in the forward problem to avoid inverse crime. In addition, image reconstructions obtained by Landweber, Newton-Raphson and Tikhonov methods are performed and used for comparison. Mathematical equations for each compared method are expressed as.

Tikhonov method:

$$F(g) = \|Sg - H\|^2 + \lambda_T \|g\|^2 \tag{16}$$

Landweber method:

$$g^{m+1} = g^m - \|S\|_2^{-2} S^{\mathrm{T}}(Sg^m - H) \tag{17}$$

Newton-Raphson method:

$$g^{m+1} = g^m - \|S\|_2^{-2} S^{\mathrm{T}}(Sg^m - H) \tag{18}$$

where λ_T denotes the regularization parameter for Tikhonov method which is determined by empirical method. By setting the parameter in a certain range, repetitive calculation is conducted until satisfactory reconstruction is obtained and the optimal regularization parameter is then determined.

In the study, six different models are reconstructed. The inclusion in the models has the same conductivity. These models cover inclusions with different quantities, different sizes and different locations. In model 1, an inclusion with the diameter of 8 mm is placed close to Electrode 4. In model 2, two inclusions with the diameter of 8 mm are respectively positioned near Electrode 4 and Electrode 10. In model 3, the larger inclusion has the diameter of 14 mm and is placed close to Electrode 4 while the smaller inclusion with the diameter of 10 mm is near Electrode 10. In model 4 and model 5, three and four inclusions with the diameter of 8 mm are separately uniformly positioned. In model 6, an inclusion with the diameter of 12 mm is positioned in the center. Images reconstructed by the TFVR method are shown in Fig. 2. During reconstruction, the conductivity of the inclusion and the background has been respectively normalized to 1 and 0. Also, the reconstruction is compared with results of Landweber, Newton-Raphson and Tikhonov methods.

From Fig. 2, it can be observed that the quality of images reconstructed by Landweber method is the worst. The reconstructed inclusion tends to be much larger than the original object. For models when there are multiple inclusions in the detected region, the boundary of inclusions can not be clearly identified from the reconstructed image. Moreover, the solution is not very accurate because this method is semi-convergent and the optimal solution may not be found. Compared with Landweber method, images reconstructed by Newton-Raphson method are generally improved. The boundary is clearer and it is easier to identify the boundary between inclusions. Images recovered by Tikhonov method are similar with the results of Newton-Raphson method. However, it takes much less time for the reconstruction with Tikhonov method. Note that inclusions are still not well reconstructed and there are obvious artifacts in the reconstructed images. Comparatively, images reconstructed by the proposed TFVR method have been largely improved. The inclusion is the most accurately reconstructed among the four methods. Moreover, the boundary of the inclusion is the clearest and almost no artifact is observed in the background.

For quantitative estimation of the proposed method in the reconstruction, blur radius (BR) is introduced to evaluate artifacts. It is defined as

$$BR = \sqrt{\frac{A_0}{A}} \tag{19}$$

where A_0 is the area of the reconstructed inclusion and A is the whole detected area [34].

Table 1 compares the calculated BR values when the reconstruction

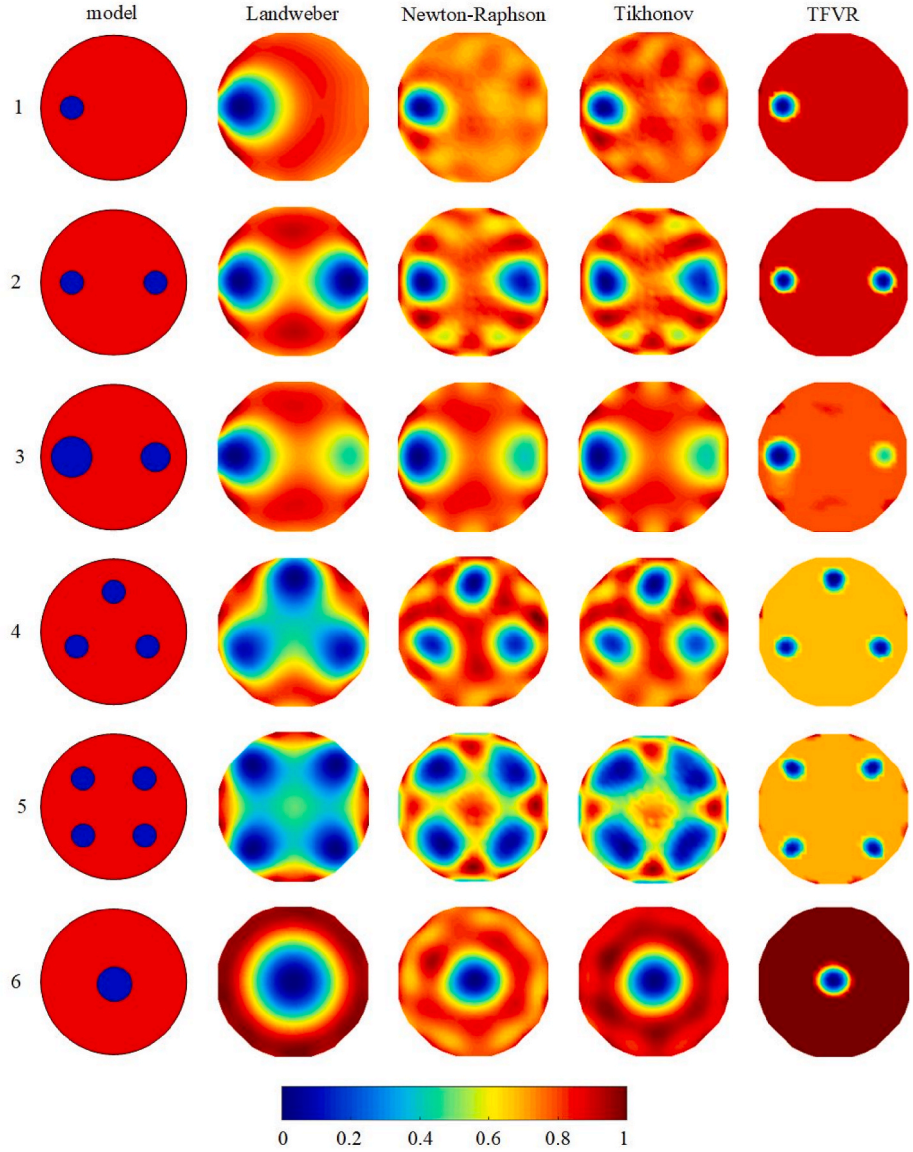

Fig. 2. Image reconstruction of different models without noise.

Table 1
Comparison of blur radius values with different methods.

Method model	Landweber	Newton-Raphson	Tikhonov	TFVR
1	0.4312	0.3747	0.3562	0.1823
2	0.5830	0.5264	0.5000	0.2301
3	0.5061	0.4629	0.4508	0.2506
4	0.7681	0.6248	0.6058	0.2579
5	0.8773	0.6714	0.6452	0.2741
6	0.5702	0.4938	0.4799	0.2046

is conducted with the four methods. From (19), it can be found that a smaller BR value indicates fewer artifacts and higher reconstruction quality. Among the four methods, the proposed method shows the lowest BR values for all the six models. It further proves the excellent performance of this method in image reconstruction.

In addition, correlation coefficient (CC) and relative error (Re) are also introduced to quantitatively describe the reliability of the proposed method in reconstructing circular inclusions with different size. Note that CC and Re respectively represents similarity and difference between the reconstructed image and the real image which are calculated as [35].

$$\mathrm{CC} = \frac{\sum_{e=1}^{t}\left(g_c^e - \overline{g}_c\right)\left(g_a^e - \overline{g}_a\right)}{\sqrt{\sum_{e=1}^{t}\left(g_c^e - \overline{g}_c\right)^2 \sum_{e=1}^{t}\left(g_a^e - \overline{g}_a\right)^2}} \tag{20}$$

$$\mathrm{Re} = \frac{\|g_c - g_a\|_2^2}{\|g_a\|_2^2} \tag{21}$$

where g_c represents calculated conductivity, g_a is actual conductivity, t is the number of pixels of g_c, g_c^e and g_a^e is the eth elements of g_c and g_a, $\overline{g}_c$and $\overline{g}_a$are the average of g_c and g_a.

Comparison of CC and Re values under noiseless condition is tabulated in Table 2. It can be found that the largest CC and the smallest Re can be obtained with the proposed method. The results demonstrate that the TFVR method is more reliable when used to reconstruct conductivity distribution.

It is also of great importance to estimate computing time of the image reconstruction method. In Table 3, time performance of Landweber, Newton-Raphson and Tikhonov methods and the proposed method are compared. It can be found that Newton-Raphson method takes the longest time as multiple iterations are required. The proposed method shows a significant improvement in reconstruction time over Landweber and Newton-Raphson methods. Since Tikhonov method requires no iteration, calculation time of the proposed method is a little longer than Tikhonov method. Although non-iterative Tikhonov algorithm is preferred for the reconstruction time, its reconstruction quality is very poor which may be suitable for rough estimation of dynamic process. However, in some industrial processes, it requires to calculate fraction of different phases. For such cases, reconstruction quality is also the focus of study. Therefore, reconstruction quality and time performance are both important for an image reconstruction algorithm. Besides, computing time of the proposed method would be reduced if a computer with higher performance is adopted.

Table 2
CC and Re values under noiseless condition.

Model	Landweber	Newton-Raphson	Tikhonov	TFVR
	CC/Re	CC/Re	CC/Re	CC/Re
1	0.4480/0.3813	0.5430/0.3352	0.5276/0.3418	0.7251/0.1528
2	0.4291/0.4143	0.5314/0.4046	0.5144/0.4078	0.7203/0.1714
3	0.6026/0.3460	0.6597/0.3210	0.6788/0.3084	0.7700/0.2451
4	0.4784/0.5231	0.5241/0.4645	0.4856/0.4689	0.5426/0.3696
5	0.4434/0.5401	0.4966/0.4942	0.4551/0.5323	0.5178/0.4174
6	0.5458/0.3488	0.7218/0.2311	0.6718/0.2598	0.8577/0.1372

Table 3
Comparison of time performance with different methods.

Method model	Landweber	Newton-Raphson	Tikhonov	TFVR
1	0.1467	0.4681	0.0128	0.0828
2	0.1392	0.4560	0.0126	0.0809
3	0.1358	0.4630	0.0138	0.0817
4	0.1345	0.4592	0.0142	0.0810
5	0.1355	0.4655	0.0129	0.0825
6	0.1383	0.4551	0.0132	0.0803

It is known that it is difficult to reconstruct inclusions with different conductivity. Aside from reconstruction of inclusions with the same conductivity, it is also essential to study the performance of the proposed method in reconstructing inclusions with different conductivity. Fig. 3 shows reconstruction of a model with the four methods. In this model, two inclusions respectively having the conductivity of 0.001 S/m and 0.005 S/m are positioned in the detected region. As can be seen from Fig. 3, the image reconstructed by the proposed method is obviously much better than other three regularization methods. The inclusion is the most accurately reconstructed. Also, the background is the clearest and no artifacts are observed.

It should be noted that noise has a large impact on the measurement. To evaluate the anti-noise performance of the proposed TFVR method in the image reconstruction, Gaussian white noise with a noise level of 1% is considered to simulate a practical system. Under the effect of noise, reconstruction result is shown in Fig. 4. It is obvious that images reconstructed by the four methods are affected by the noise. In some reconstructions, the recovered inclusions are deformed and more artifacts are observed. Nevertheless, the TFVR method proposed in this work shows the strongest robustness to the noise among the four methods. The inclusion is still the best reconstructed and the background shows the fewest artifacts.

Under the noise level of 1%, Table 4 compares the BR values when reconstruction of six models is performed with the four methods. Again, the proposed TFVR method shows the smallest BR value among these methods which further demonstrates the robustness of this method to noise.

For the six models under the noise level of 1%, comparison of CC and Re values is given in Table 5. Compared with the results under noiseless condition, CC becomes smaller while Re gets larger. Nevertheless, the proposed TFVR method still shows its better anti-noise performance than other three methods.

In addition, Fig. 5 shows the anti-noise performance of the proposed TFVR method in reconstructing inclusion with different conductivity. Reconstructed images are compared with the results obtained by Landweber, Newton-Raphson and Tikhonov methods. It is found that shape of inclusions can be much better reconstructed by the TFVR method and reconstruction is less affected by noise. Comparatively, serious deformation of inclusions is generated and lots of artifacts are observed in the reconstructed images of other three methods.

4.2. Phantom experimental validation

To validate the feasibility and effectiveness of the proposed TFVR image reconstruction algorithm, we carried out phantom experiments on a 12-electrode CCERT system in our laboratory [36]. A tank with inner and outer diameter of respectively 106 mm and 110 mm is filled by tap water with the conductivity of 0.018 S/m. Twelve electrodes with the angle of 25° are equidistantly arranged outside the tank. Several combinations of plastic rods with the diameter of 26.5 mm, 29.5 mm and 34.5 mm are employed as the inclusion. In the experiment, the temperature is 24 °C. Data acquisition frame rate is 30 frames/s. The frequency and amplitude of the excitation voltage are 500 kHz and 3.3V respectively. By injecting an AC voltage into an excitation electrode, current reflecting conductivity of sensing area can be successively

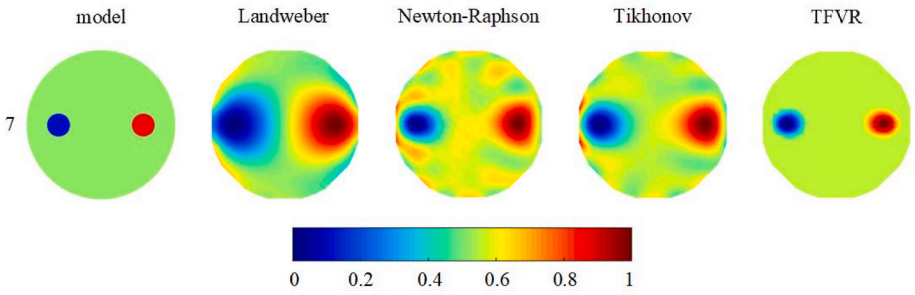

Fig. 3. Reconstruction of a model with inclusions having different conductivity.

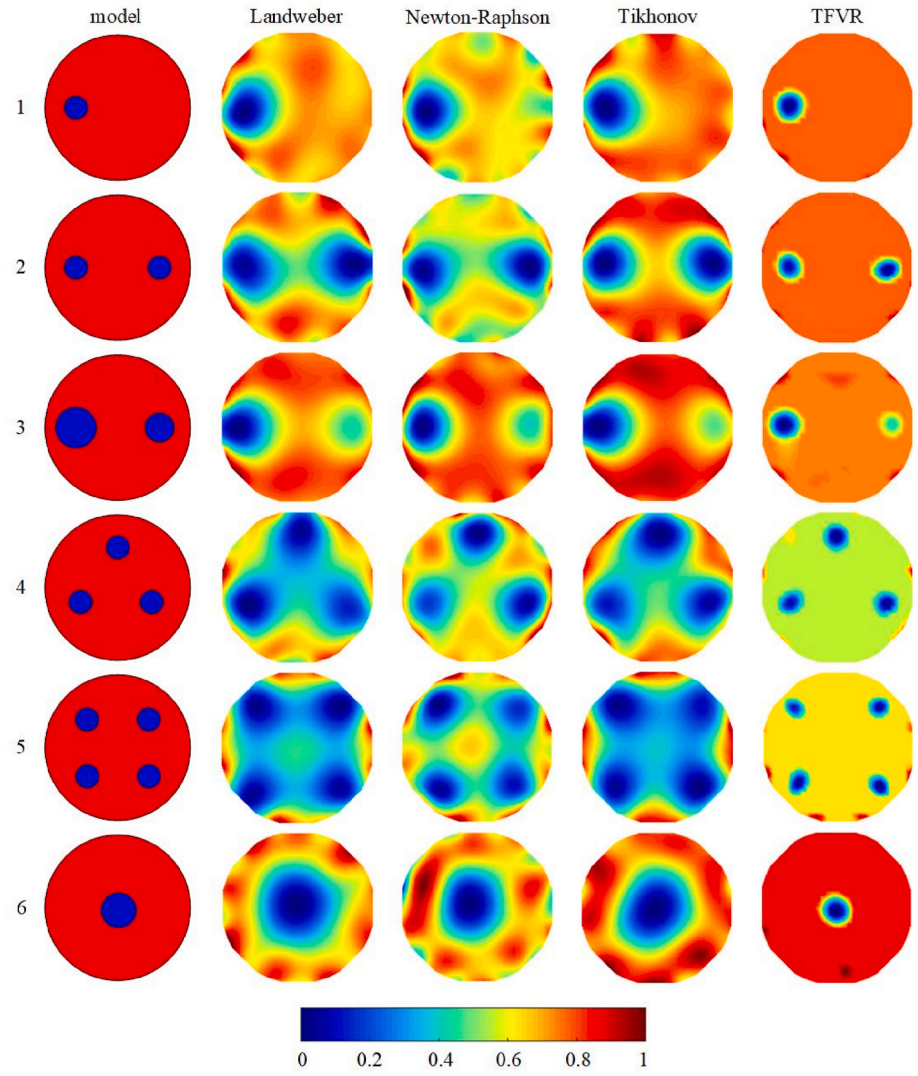

Fig. 4. Image reconstruction under noise level of 1%.

Table 4
Comparison of blur radius values under noise level of 1%.

Method model	Landweber	Newton-Raphson	Tikhonov	TFVR
1	0.4773	0.4589	0.4298	0.1683
2	0.6099	0.5659	0.5648	0.2135
3	0.5205	0.5000	0.4988	0.2163
4	0.7728	0.6058	0.7453	0.2531
5	0.8710	0.7616	0.8200	0.2718
6	0.6877	0.6078	0.6209	0.1985

obtained on the detection electrode. The measurement cycle continues until each electrode has been selected as excitation electrode. For a 12 electrodes CCERT system, a total of 66 independent measurements are then obtained. Fig. 6 shows reconstruction results. Also, comparison is made with the images reconstructed by Landweber, Newton-Raphson and Tikhonov methods. From Fig. 6, it can be observed that the proposed TFVR method outperforms other three methods during the reconstruction of conductivity distribution. The reconstructed object is the most similar with the true inclusion. Furthermore, the boundary of inclusions is the clearest and the artifacts in the background are the

Table 5
The values of Re and CC under noise level of 1%.

Model	Landweber	Newton-Raphson	Tikhonov	TFVR
	CC/Re	CC/Re	CC/Re	CC/Re
1	0.4405/0.3976	0.4870/0.3839	0.4159/0.3995	0.7156/0.1693
2	0.4182/0.4332	0.4952/0.4172	0.4450/0.4126	0.6913/0.3106
3	0.5911/0.3627	0.6081/0.3434	0.5747/0.3716	0.6480/0.3135
4	0.4614/0.5859	0.5015/0.4851	0.4923/0.4905	0.5317/0.3781
5	0.4331/0.5523	0.4850/0.5042	0.4402/0.5348	0.5059/0.4185
6	0.5029/0.4597	0.5833/0.3877	0.5451/0.4203	0.7749/0.2377

least. Although the laboratory scenario is a bit different when measuring with pumps and motors working around, clear images can still be reconstructed if effective shielding measures are taken to protect the EIT equipment from noise interruption.

5. Conclusion

In this paper, a novel TFVR method is proposed for recovering conductivity distribution in CCERT. According to the measurement principle, the mathematical model of CCERT is firstly established. To acquire conductivity distribution, iterative alternating minimization scheme is adopted to solve the proposed method. To verify the performance of the proposed TFVR strategy, reconstruction of several typical models with inclusions having the same conductivity is studied by simulation work. An additional model with inclusions having different conductivity is also studied. The results show that images reconstructed by the proposed method are obviously much better than other three regularization methods. By introducing the concept of blur radius, quantitative evaluation of the proposed method in inhibiting artifacts is conducted. It is found that BR values of the proposed method are the lowest which indicates the fewest artifacts and highest reconstruction quality. Additionally, reliability of the proposed method is also quantitatively validated by CC and Re values. Calculation time of the proposed method

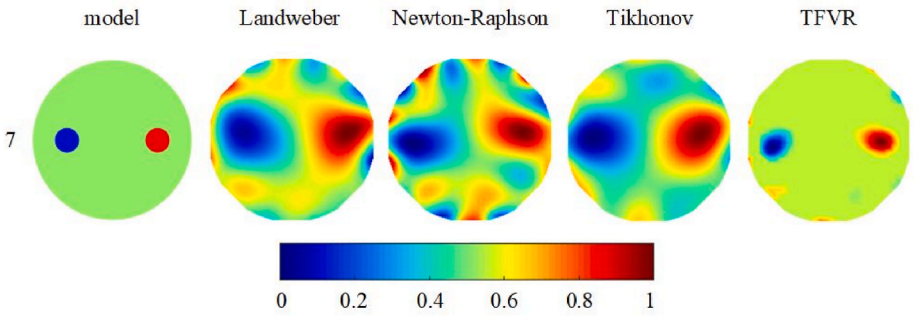

Fig. 5. Image reconstruction of inclusions with different conductivity under noise level of 1%.

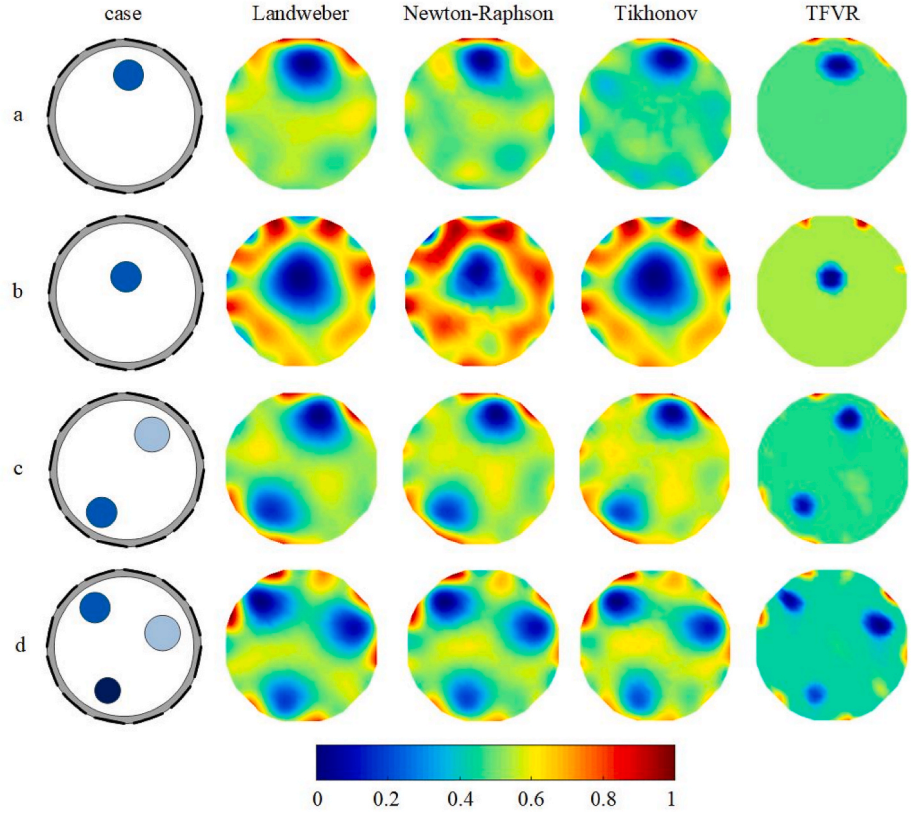

Fig. 6. Reconstructed images based on experimental cases.

is acceptable. Furthermore, anti-noise performance of the four methods is compared and the strongest robustness to noise is observed for the proposed TFVR method. Phantom experiments demonstrate the effectiveness of the proposed method. Therefore, the proposed method can be considered as a promising candidate for reconstruction of conductivity distribution in CCERT.

Author statement

Yanyan Shi: Conceptualization, Methodology; Juanjuan Liao: Software, Writing – original draft; Meng Wang: Supervision; Feng Fu: Supervision; Yating Li: Visualization; Manuchehr Soleimani: Writing-Reviewing and Editing.

Declaration of competing interest

The authors declared that they have no conflicts of interest to this work.

Acknowledgement

This work is supported in part by National Natural Science Foundation of China under Grant 61903127 and 51837011, in part by Postdoctoral Research Foundation of China under Grant 2020M673664, in part by Scientific and Technological Innovation Program for Universities in Henan Province of China under Grant 21HASTIT018 and in part by Foundation for University Key Young Teacher by Henan Province of China under Grant 2020GGJS061.

References

[1] R. Kotze, A. Adler, A. Sutherland, C.N. Deba, Evaluation of electrical resistance tomography imaging algorithms to monitor settling slurry pipe flow, Flow Meas. Instrum. 68 (2019) 101572.
[2] H.R. Wang, J.B. Jia, Y.J. Yang, et al., Quantification of gas distribution and void fraction in packed bubble column using electrical resistance tomography, IEEE Sensor. J. 18 (21) (2018) 8963–8970.
[3] G. Annamalai, S. Pirouzpanah, S.R. Gudigopuram, G.L. Morrison, Characterization of flow homogeneity downstream of a slotted orifice plate in a two-phase flow using electrical resistance tomography, Flow Meas. Instrum. 50 (2016) 209–215.
[4] M.A. Sattar, M.M. Garcia, R. Banasiak, et al., Electrical resistance tomography for control applications: quantitative study of the gas-liquid distribution inside a cyclone, Sensors 20 (21) (2020) 6069.
[5] F. Maluta, G. Montante, A. Paglianti, Analysis of immiscible liquid-liquid mixing in stirred tanks by Electrical Resistance Tomography, Chem. Eng. Sci. 227 (2020) 115898.
[6] P.C. Hauser, P. Kuban, Capacitively coupled contactless conductivity detection for analytical techniques - developments from 2018 to 2020, J. Chromatogr. A 1632 (2020) 461616.
[7] Y.X. Wang, B.L. Wang, Z.Y. Huang, et al., New capacitively coupled electrical resistance tomography (CCERT) system, Meas. Sci. Technol. 29 (10) (2018) 104007.
[8] S.J. Ren, Y. Wang, G.H. Liang, F. Dong, A robust inclusion boundary reconstructor for electrical impedance tomography with geometric constraints, IEEE Trans. Instrum. Measure. 68 (3) (2019) 762–773.
[9] F. Li, C. Tan, F. Dong, Electrical resistance tomography image reconstruction with densely connected convolutional neural network, IEEE Trans. Instrum. Measure. 70 (2021) 4500811.
[10] S.J. Ren, K. Sun, D. Liu, F. Dong, A statistical shape constrained reconstruction framework for electrical impedance tomography, IEEE Trans. Med. Imag. 38 (10) (2019) 2400–2410.
[11] Y.Y. Shi, X. Zhang, Z.G. Rao, Reduction of staircase effect with total generalized variation regularization for electrical impedance tomography, IEEE Sensor. J. 19 (21) (2019) 9850–9858.
[12] B.L. Wang, W.H. Tan, Z.Y. Huang, et al., Image reconstruction algorithm for capacitively coupled electrical resistance tomography, Flow Meas. Instrum. 40 (2014) 216–222.
[13] W.H. Tan, B.L. Wang, Z.Y. Huang, et al., New image reconstruction algorithm for capacitively coupled electrical resistance tomography, IEEE Sensor. J. 17 (24) (2017) 8234–8241.
[14] Y.X. Wang, H.F. Ji, Z.Y. Huang, et al., Study on image reconstruction of capacitively coupled electrical impedance tomography (CCEIT), Meas. Sci. Technol. 30 (9) (2019), 094002.
[15] Y.B. Xu, Y. Pei, F. Dong, An adaptive Tikhonov regularization parameter choice method for electrical resistance tomography, Flow Meas. Instrum. 50 (2016) 1–12.
[16] X.Z. Song, Y.B. Xu, F. Dong, A hybrid regularization method combining Tikhonov with total variation for electrical resistance tomography, Flow Meas. Instrum. 46 (2015) 268–275.
[17] Y.Y. Shi, Z.G. Rao, C. Wang, et al., Total variation regularization based on iteratively reweighted least-squares method for electrical resistance tomography, IEEE Trans. Instrum. Measure. 69 (6) (2020) 3576–3586.
[18] B. Chen, J.F.P.J. Abascal, M. Soleimani, Electrical resistance tomography for visualization of moving objects using a spatiotemporal total variation regularization algorithm, Sensors 18 (6) (2018) 1704.
[19] Y.J. Yang, H.C. Wu, J.B. Jia, Image reconstruction for electrical impedance tomography using enhanced adaptive group sparsity with total variation, IEEE Sensor. J. 17 (17) (2017) 5589–5598.
[20] A. Javaherian, M. Soleimani, K. Moeller, et al., An accelerated version of alternating direction method of multipliers for TV minimization in EIT, Appl. Math. Model. 40 (21–22) (2016) 8985–9000.
[21] Y.Y. Shi, X.L. Kong, M. Wang, et al., A non-convex L_1-norm penalty-based total generalized variation model for reconstruction of conductivity distribution, IEEE Sensor. J. 20 (14) (2020) 8137–8146.
[22] H.L. Zhang, L.M. Tang, Z. Fang, et al., Nonconvex and nonsmooth total generalized variation model for image restoration, Signal Process. 143 (2018) 69–85.
[23] P.F. Liu, Hybrid higher-order total variation model for multiplicative noise removal, IET Image Process. 14 (5) (2020) 862–873.
[24] J.H. Yang, X.L. Zhao, T.H. Ma, et al., Remote sensing images destriping using unidirectional hybrid total variation and nonconvex low-rank regularization, J. Comput. Appl. Math. 363 (2020) 124–144.
[25] M. Henriques, D. Valerio, P. Gordo, R. Melicio, Fractional-order colour image processing, Mathematics 9 (5) (2021) 457.
[26] Y.X. Wang, X.K. He, Y.D. Jiang, et al., New image reconstruction algorithm for CCERT: LBP plus Gaussian mixture model (GMM) clustering, Meas. Sci. Technol. 32 (2) (2021), 024001.
[27] Y.D. Jiang, X.K. He, B.L. Wang, et al., On the performance of a capacitively coupled electrical impedance tomography sensor with different configurations, Sensors 20 (20) (2020) 5787.
[28] B.L. Wang, W.B. Zhang, Z.Y. Huang, et al., Modeling and optimal design of sensor for capacitively coupled electrical resistance tomography system, Flow Meas. Instrum. 31 (2013) 3–9.
[29] Y.D. Jiang, M. Soleimani, B.L. Wang, Contactless electrical impedance and ultrasonic tomography: correlation, comparison and complementarily study, Meas. Sci. Technol. 30 (11) (2019) 114001.
[30] S. Bartels, M. Milicevic, Efficient iterative solution of finite element discretized nonsmooth minimization problems, Comput. Math. Appl. 80 (5) (2020) 588–603.
[31] J.C. Bai, Y.X. Ma, H. Sun, M. Zhang, Iteration complexity analysis of a partial LQP-based alternating direction method of multipliers, Appl. Numer. Math. 165 (2021) 500–518.
[32] J.J. Zhang, J.G. Nagy, An effective alternating direction method of multipliers for color image restoration, Appl. Numer. Math. 164 (2021) 43–56.
[33] H.C. Zhang, W.W. Hager, A nonmonotone line search technique and its application to unconstrained optimization, SIAM J. Optim. 14 (4) (2004) 1043–1056.
[34] A. Adler, J.H. Arnold, R. Bayford, et al., GREIT: a unified approach to 2D linear EIT reconstruction of lung images, Physiol. Meas. 30 (6) (2009) S35–S55.
[35] Y.Y. Shi, Q.F. Li, M. Wang, et al., A non-convex regularization method combined with Landweber method for image reconstruction in electrical resistance tomography, Flow Meas. Instrum. 79 (2021) 101917.
[36] Z.R. Chen, G.G. Ma, Y.D. Jiang, et al., Application of deep neural network to the reconstruction of two-phase material imaging by capacitively coupled electrical resistance tomography, Electronics 10 (2021) 1058.